ELSEVIER

Marine Geology 216 (2005) 17–26

MARINE GEOLOGY
INTERNATIONAL JOURNAL OF MARINE GEOLOGY, GEOCHEMISTRY AND GEOPHYSICS

www.elsevier.com/locate/margeo

In situ measurement of electrical resistivity of marine sediments, results from Cascadia Basin off Vancouver Island

Daniela Jansen*[,1], Bernd Heesemann, Marion Pfender, Andreas Rosenberger[2], Heinrich Villinger

Department of Geosciences, University of Bremen, Klagenfurter Straße, 28359 Bremen, Germany

Received 5 April 2004; received in revised form 5 November 2004; accepted 4 February 2005

Abstract

Electrical properties of sediments encompass information about other linked physical properties, such as porosity and thermal conductivity. In situ measurements of electrical resistivity offer a cost- and time effective method for obtaining a comprehensive overview of near surface sediment physical properties. They also provide a quality check for in situ measurements of related sediment properties or for data obtained from sediment core analysis.

We present results from the deployment of a sediment penetrating in situ probe which logs electrical resistivity of marine or limnic sediments up to 4 mbsf. Additionally, acceleration and pressure are recorded during sediment penetration. As the integration of acceleration delivers penetration depth with respect to time, a resistivity–depth profile can be derived.

The measurements presented were performed during cruise SO-149 in the Cascadia Basin and at the eastern flank of the Juan de Fuca Ridge. The in situ probe is attached to a Lister-type heat flow instrument; therefore simultaneous measurements of thermal and electrical resistivities are possible. Strongly influenced by porosity, both data sets show good correlation. Continuous recordings of electrical resistivity can be used to validate and supplement the thermal data, which is only measured in depth intervals of 30 cm. Comparison with other independent measurements such as porosity measured on sediment cores also confirm the correct operation of the probe.

Keywords: electrical resistivity; thermal conductivity; porosity; marine sediments; in situ probe; physical properties

1. Introduction

The electrical properties of deep sea sediments are linked to other sediment properties through various physical processes. An interesting parameter in marine geoscience and engineering is, for example, the porosity of sediments, which can be determined

* Corresponding author. Tel.: +49 471 4831 1874; fax: +49 471 4831 1797.
E-mail address: djansen@awi-bremerhaven.de (D. Jansen).
[1] Present Address: Alfred Wegener Institute Foundation for Polar and Marine Research, Bussestrasse 24, 27570 Bremerhaven, Germany.
[2] Present Address: Pacific Geoscience Centre, Sidney, B. C., Canada.

0025-3227/$ - see front matter © 2005 Elsevier B.V. All rights reserved.
doi:10.1016/j.margeo.2005.02.002

from electrical resistivity by means of Archie's Law (Archie, 1942). A commonly used method of surveying physical properties is the coring and analysis of the cored sediments in the laboratory. However, the change in temperature and in pressure while lifting the sediment core aboard, or during storage, can influence the sediment properties. Therefore it is of advantage to determine sediment properties under in situ conditions. In this paper we present results obtained using an in situ electrical resistivity probe for the uppermost 4 m of deep sea sediment. The primary purpose of this instrument was to complement and validate thermal conductivity measurements, and it is thus attached to a Lister-type heat flow probe (Hyndman et al., 1979). In addition, the probe can be deployed separately allowing the mapping of surficial sediment porosities at comparatively low cost.

In the following a short introduction of the construction and measurement principle will be given, for details see Rosenberger et al. (1999). We will focus on presenting the data and on comparison and validation of this electrical data with independent measurements like thermal conductivity and porosity of sediment cores.

The data presented were collected in the summer of 2000 during cruise SO-149 of the German R/V "*Sonne*". The aim of SO-149 was to investigate different types of suspected fluid flow regimes at the eastern flank and the active part of the Juan de Fuca Ridge and in the Cascadia basin. During the cruise physical properties of sediments were mapped acoustically in attempt to quantify exchanges between ocean and sediment and to detect possible lateral gradients (Spieß and Fahrtteilnehmer, 2001). In particular, in situ measurements were carried out to substantiate a seismic survey from a previous cruise of R/V "*Sonne*", SO-111, in which narrow zones of low seismic reflection were observed and associated with low porosity values (Zühlsdorff et al., 1999).

2. Working area

The working area of SO-149 was the Cascadia Basin, which extends from the western continental margin of Canada, Vancouver Island, to the Juan de Fuca Ridge several hundreds of kilometers west of the coastline. The ridge forms a barrier for terrigenous sediments transported across the continental slope. Therefore the basin is filled with turbiditic sediments and even the eastern flank of the ridge is fully covered with sediment (Shipboard Scientific Party, 1997). In this area measurements were carried out on several profiles at locations with different conditions of sedimentation and sea floor morphology (Fig. 1).

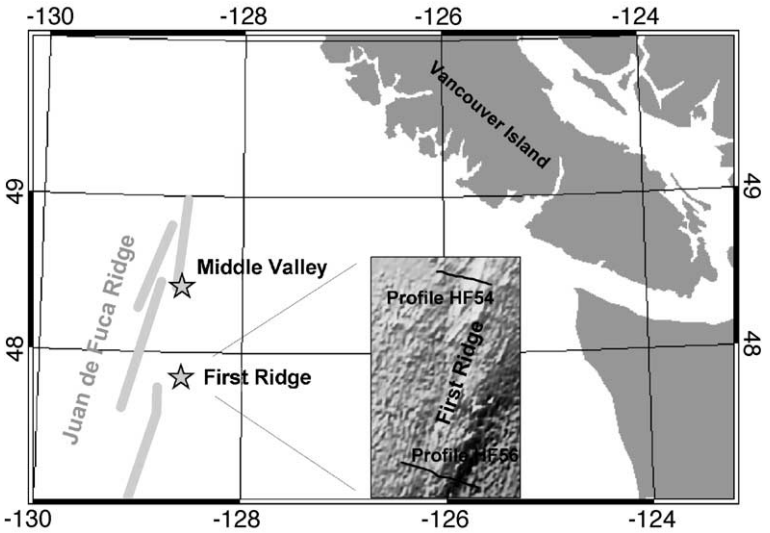

Fig. 1. An overview of the working area. Sea floor topography: personal communication L. Zuehlsdorff, University of Bremen, Germany.

The oceanic crust at the eastern flank of the Juan de Fuca Ridge shows a sequence of alternating ridges and troughs parallel to the main ridge, which are due to normal faulting and variations in volcanic supply during formation of the crust (Kappel and Ryan, 1986). The first ridge, which is fully covered with sediments, is located 40 km east of the actual ridge on 1.4 Ma old crust (Davis and Villinger, 1992). The sediment cover varies from 20 to 150 m, while the sea floor topography reflects the basement structure (Spieß and Fahrtteilnehmer, 2001). Perpendicular to this ridge, in the following referred to as First Ridge, profiles of electrical and thermal data were surveyed.

The Juan de Fuca Ridge consists mainly of narrow axial rift zones, split in segments of about 50- to 100-km length. This morphology resembles typical moderate to fast spreading ridges (Davis and Villinger, 1992). In the northern part of the ridge the spreading zone consists of three axial deep valleys: West Valley, Endeavor Valley and Middle Valley (e.g. McManus et al., 1972). Middle Valley is filled with hemipelagic and turbiditic sediments, and sediment cover partly reaches a thickness of 2 km (Shipboard Scientific Party, 1992). At this location two profiles of electrical resistivity were surveyed.

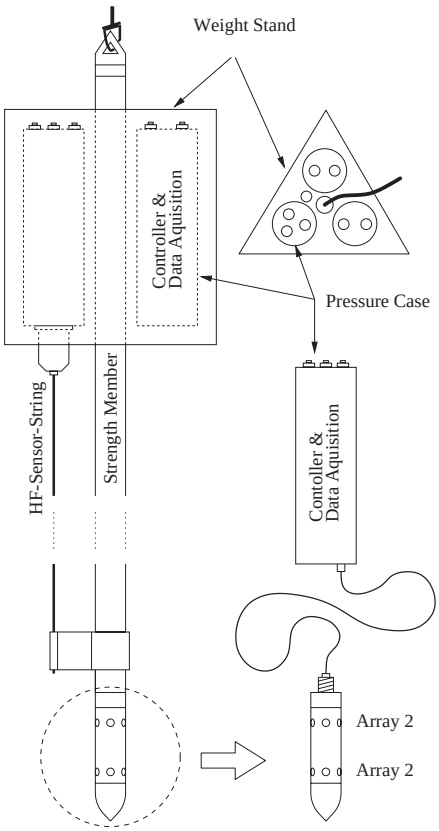

Fig. 2. The resistivity tip (circled) is part of a Lister type heat probe. The strength member carries a 500-kg weight stand of triangular shape. The electronics are placed in pressure cases which can be fixed inside of the weight stand (Rosenberger et al., 1999).

3. Construction and measurement principle

As described in Rosenberger et al. (1999) the in situ probe is fitted to a Lister-type heat flow instrument (Hyndman et al., 1979), comprising a 500 kg weight stand which also houses the pressure cases of the data loggers (Fig. 2). The electrical sensing array is mounted at the tip of the violin bow strength member. Tip and head of the probe are made of steel and connected with a steel bolt to provide inner stability (Fig. 3). Two electrode arrays constructed from sea water grade bronze are embedded in a cylindric covering of delrin, a non-conducting, non abrasive plastic material very stable under high pressure conditions. The interior void between bolt and covering is filled with polyurethane, so that the probe hardly needs any maintenance.

The two electrode arrays are operated independently, thus providing an instant test of repeatability. Due to a vertical spacing of 10 cm between them, resistivity features are measured at different times by the upper and lower array. Therefore, penetration velocity can be estimated from these two profiles. Since each electrode array consist of two current electrodes and four potential electrodes, the arrangement resembles two Wenner type configurations projected onto a half cylinder (Fig. 4). To compensate small scale lateral changes in resistivity, the potential electrodes of the opposite Wenner configurations are connected and deliver an average voltage.

The current electrodes are fed by an alternating DC current with a frequency of 500 Hz. The two arrays alternate during each cycle, which leads to a sample rate of 250 Hz for the voltage difference between the potential electrodes. The recorded value represents the RMS value of ten samples. To monitor the penetration process, the probe includes an acceleration sensor and

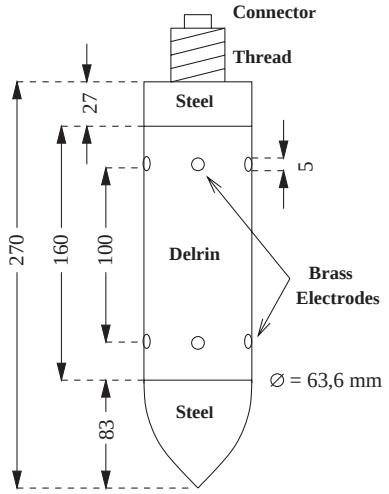

Fig. 3. An enlarged view of the resistivity probe. The electrodes are embedded in a non conducting plastic material, tip and head of the probe are made of steel and are connected with a steel bolt to provide inner stability (Rosenberger et al., 1999).

a pressure sensor. Both parameters are also sampled with a frequency of 250 Hz.

An additional function of the pressure sensor is to control data acquisition. Before deployment of the probe a pressure threshold value has to be chosen. If the measured value exceeds the predetermined threshold, data recording will begin, and end when the value drops below. In this way the amount of data which is to be stored is reduced and "pogo" style measurements are enabled: the probe is lifted back on board only at the end of a profile, whereas it is just lifted for several hundred meters above the sea floor between single penetrations (Hyndman et al., 1979).

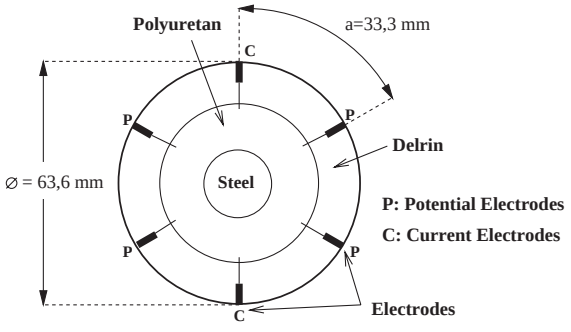

Fig. 4. A cut through the resistivity probe. The electrode arrangement resembles two Wenner type arrays projected onto a cylinder surface (Rosenberger et al., 1999).

4. Data processing

As a first step, the single penetrations of the probe have to be extracted from the continuous data record. Beginning and end of the sediment penetrating process are marked by sudden changes on all data channels. High amplitudes in acceleration data are a characteristic indication for the weight stand hitting the sea floor (Fig. 5).

Penetration depth vs. time is obtained by two-fold integration of acceleration. The acceleration sensor is

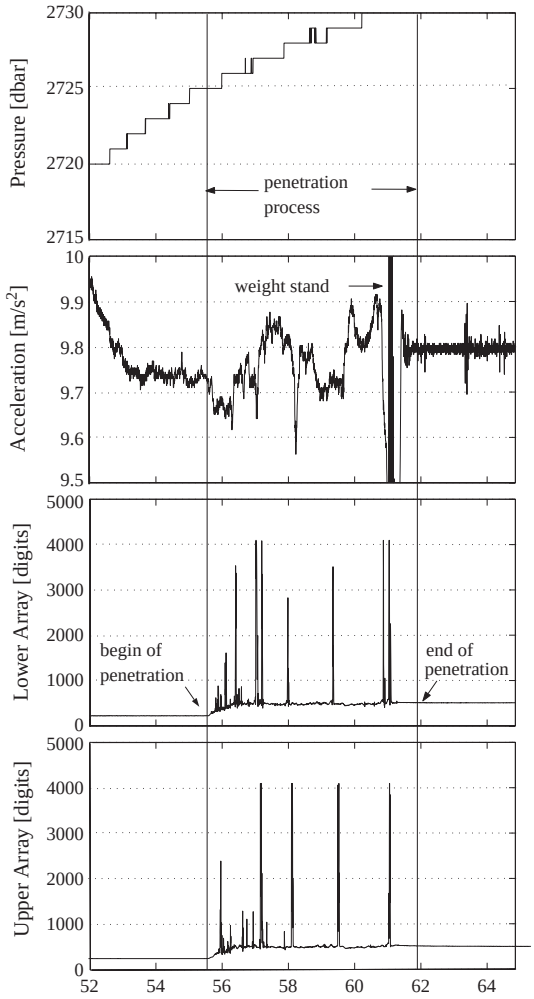

Fig. 5. Raw data of a typical penetration process (Profile 54, First Ridge, Penetration 5). Begin and end of the penetration are marked by sudden changes on all data channels. High amplitudes in acceleration data are characteristic for the weight stand hitting the sea floor.

not calibrated absolutely, and hence the calculated penetration depth is normalized to a thermal penetration depth which can be derived from the thermal data measured by the heat flow probe. Thermal penetration depth is based on Bullard (1939):

$$T(z) = q \int_0^z \frac{\mathrm{d}z^*}{\lambda(z^*)} + T_0 \quad (1)$$

where T_0 is the bottom water temperature, λ the thermal conductivity and q the heat flow. The integral is known as thermal resistance or Bullard depth. The thermal conductivity profile is measured with the pulsed line source method (Lister, 1979). The complete data processing of the thermal measurements is described in detail by Hyndman et al. (1979), Villinger and Davis (1987), and Hartmann and Villinger (2002). Since the temperature sensors are 30 cm apart, the integral in Eq. (1) turns into a discrete sum. The heat flow is obtained by linear regression of temperature versus thermal resistance. The position of the uppermost thermistor relative to the sea floor can now be estimated from the average thermal conductivity and the calculated thermal resistance for which T is equal to bottom water temperature T_0. At some sites only electrical data exist. In this case the calculated penetration depth has to be normalized by the distance from the bottom of the weight stand to the tip of the probe.

The electrical data are presented as formation factor, which is defined as the ratio of total resistivity ρ to pore fluid resistivity ρ_f:

$$\mathrm{FF} = \frac{\rho}{\rho_f} \quad (2)$$

As the conductivity of porous media depends on pore fluid rather than on the isolating matrix, the formation factor provides information about sediment porosity. This relation between porosity and conductivity or resistivity was described by Archie (1942):

$$\mathrm{FF} = \frac{\rho}{\rho_f} = \frac{a}{\varphi^m} \quad (3)$$

where φ is the sediment porosity and a and m are empirical constants which depend on sediment composition and texture. Data derived from ODP-Sites 1030 and 1031 indicate, that the measurement sites are characterised by sediments with a relatively high carbonate content and little sand (Shipboard Scientific Party, 1992). Thus, we chose values for a and m determined by Boyce (1968), which were obtained from carbonate bearing to sediments of the Bering Sea: a=1.3 and m=1.45.

Porosity values obtained by Eq. (3) with these parameters show good correlation with porosities obtained from independent measurements (see next section). In all calculations it is assumed that the salinity and therefore resistivity of the pore fluid are constant and equal to bottom water salinity.

As mentioned before, porosity also affects thermal conductivity, described by an empirical formula (Brigaud and Vasseur, 1989):

$$\lambda = \lambda_f^{\varphi} \lambda_m^{1-\varphi} \quad (4)$$

were λ is thermal conductivity of the sediment, λ_f is the thermal conductivity of the pore fluid and λ_m the thermal conductivity of the sediment matrix. Therefore, porosity can also be calculated from thermal conductivity measurements, if λ_f and λ_m are known. For the data presented here we assumed a matrix conductivity of 3.2 W/mK, taken from ODP measurements during leg 139 in Cascadia Basin (Kinoshita, 1994), and a thermal conductivity of seawater with an average salinity at 0 °C of 0.5602 W/mK (Schön, 1996). Thus, the combination of a heat flow and electrical resistivity probe allows a direct comparison of porosity obtained from independent in situ data recorded at the same time, location and depth interval.

5. Results and discussion

The in situ probe for electrical resistivity was deployed during cruise SO-149 in the area of Cascadia Basin at several sites with different sea floor morphology and sedimentation conditions. In total we performed 75 successful measurements in water depths ranging from 1200 to 2600 m. The first site presented is First Ridge, where measurements have been carried out on four profiles perpendicular to the ridge structure. Fig. 6 shows formation factor of the upper and lower array vs. time during a typical penetration. The records show narrow peaks, which enclose several sample intervals. They are super-

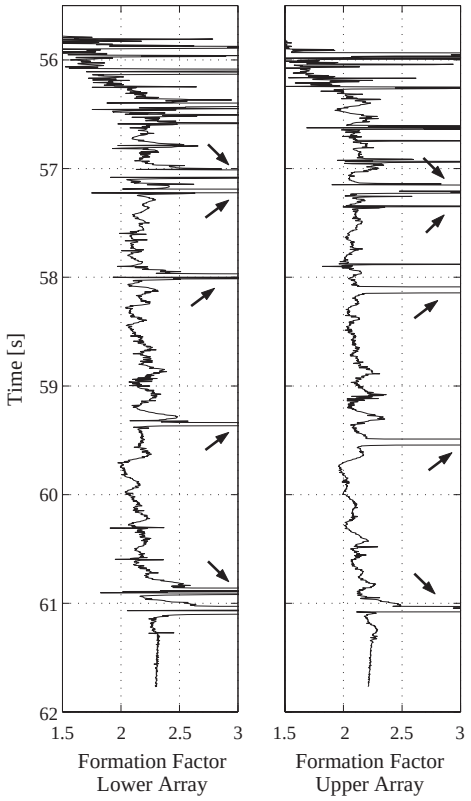

Fig. 6. Formation Factor versus time (Profile 54, First Ridge, Penetration 5). The peaks marked by arrows were used to estimate penetration velocity.

imposed on a nearly constant background value and there is a time shift between the records of upper and lower array. The fact that both arrays record the peaks at different times supports the interpretation that they are real and connected to the local sediment properties and structure. The penetration velocity estimated from the time shift and the vertical distance between the arrays is in good agreement with the velocity derived from integration (Fig. 7).

We assume that the spurious high resistivity measurements are due to an inclined penetration of the probe combined with strong porosity gradients, as inhomogenities in porosity and therefore resistivity cause a distortion of the electromagnetic field. In particular, if one current electrode is connected to a sediment layer with low resistivity and the other electrodes to a layer with higher resistivity, the measured potential difference would be too high, a problem well known from borehole measurements

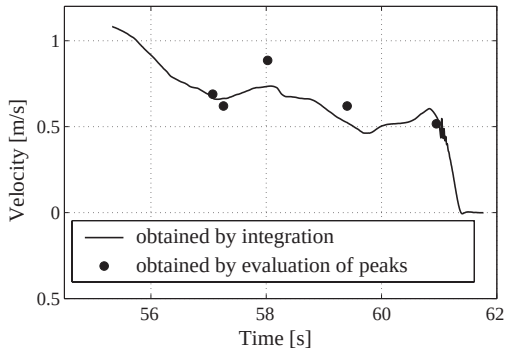

Fig. 7. Comparison of calculated penetration velocities of Profile 54, First Ridge, Penetration 5. The peaks marked in Fig. 5 were used to calculate velocities at certain times.

(e.g. Ellis, 1987). Fig. 8 shows a typical resistivity log obtained from a lateral device measurement for a thin high resistivity layer. Therefore the peaks may not be evaluated quantitatively, but they are probably an indication for strong porosity gradients. However, not all peaks are observed by both arrays, as the inclination may change during penetration.

Along with the electrical measurements, heat flow and thermal conductivity measurements were performed. In Fig. 9 a comparison of porosity derived from electrical and thermal data from the penetration shown in Fig. 5 is presented. We also included data obtained from two sediment cores taken in close vicinity (personal communication, A. Fisher, UCSC, Santa Cruz, USA). On average there is a good correlation of these independently measured data sets. Small scale variation shown in electrical data cannot be verified by core data or thermal data, as the latter

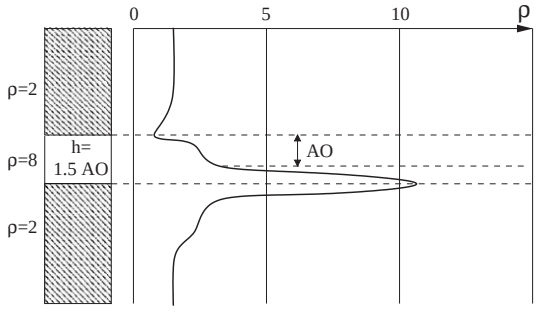

Fig. 8. A typical log for a high resistivity layer recorded by a lateral device. The measured resistivity is well above the real value. AO: distance between the lowered current electrode and the potential electrodes. From Ellis, 1987.

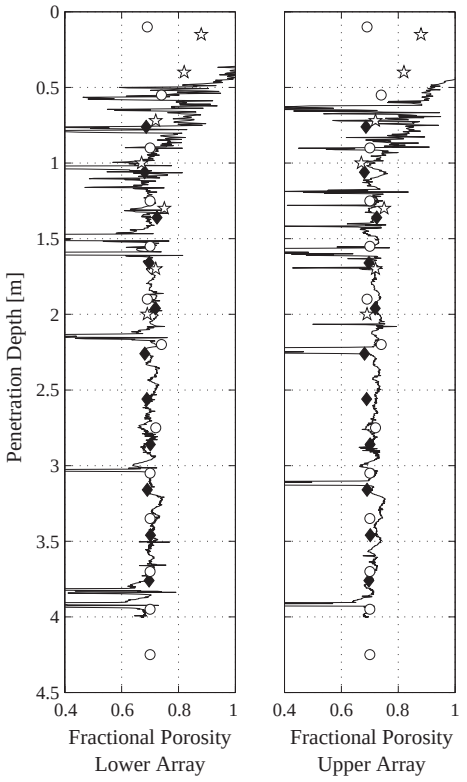

Fig. 9. Porosity versus penetration depth for Profile 54, First Ridge, Penetration 5. Compared are porosities derived from formation factor (solid line), thermal conductivity (solid diamonds), and laboratory data (open circles: piston core PC62; open stars: gravity core GC49; personal communication, A. Fisher, University Santa Cruz, USA).

are only given for discrete points in certain depth intervals. Variation of porosity, however, is of the order of about 8% in all data sets. The average value of porosity which is about 70% is in good agreement with ODP measurements near this site (Shipboard Scientific Party, 1997).

Previous seismic surveys of the First Ridge area revealed linear zones of reduced seismic reflectivity which where orientated roughly parallel to the ridge crest and associated with areas of high porosity (Zühlsdorff et al., 1999). According to Zühlsdorff and Spieß (submitted for publication), these narrow zones of deceased reflection amplitudes are clearly correlated with pronounced basement peaks, but are independent from seafloor inclination or distance from the ridge crest. As all observed blanking zones are linked with locally flexed layering, Zühlsdorff and Spiess suggest, that the vertical zones of higher porosity are related to forced folding, which is defined by Stearns (1978), as folding, in which the final overall shape and trend of the fold are dominated by the shape of some forcing member below. They further assume that the extensional stress field, which is caused by layer perpendicular shortening and layer parallel extension within forced folds (Cosgrove and Ameen, 2000), explains part of the locally high porosity in their vicinity.

To detect the expected lateral changes of sediment porosity based on resistivity measurements, median values of each penetration were calculated for both formation factor and thermal conductivity, shown in Fig. 10. The good correlation of thermal and electrical data is evident here, too. The profile starts about 2 km west of the ridge and the last penetration is positioned on the ridge crest. While the values for the formation factor and thermal conductivity are comparatively high at the beginning of the profile, there is a sudden change in the fourth penetration, after which the measurements yield lower values. The absolute change of porosity is about 7%. Another profile perpendicular to the ridge about 7 km south shows similar results (Fig. 11). However, the total increase of porosity along the profile is lower than expected. But results from several penetration indicate, that porosity is also increasing with depth (Fig. 12). This additional porosity change of about 10% is supported by the analysis of a sediment core, although the change occurs at a 1-m higher depth level here, which could

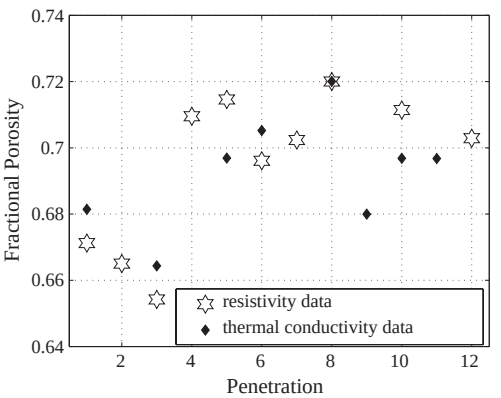

Fig. 10. Median values of porosity derived from formation factor (diamonds) and thermal conductivity (stars) of Profile 54, First Ridge, direction west to east.

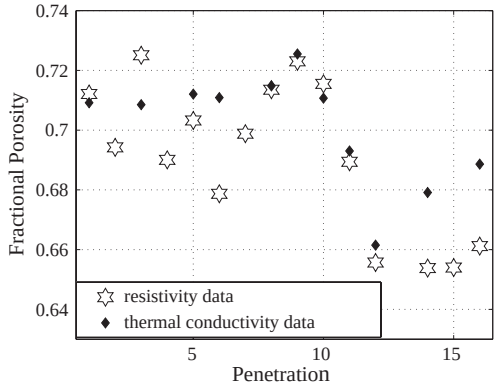

Fig. 11. Median values of porosity derived from formation factor (diamonds) and thermal conductivity (stars) of Profile 56, First Ridge, direction east to west.

be due to core loss or possibly strong lateral variation of the depth of the high porosity zone. Thus, the 4 m penetration of the in situ resistivity probe might be too short for adequate mapping of this porosity anomaly.

The relatively impermeable sediment cover over very young and hot crust above the active part of the Juan de Fuca Ridge at Middle Valley allows the thermal regimes to be characterized by heat flow measurements (Shipboard Scientific Party, 1992). For supplementation of the thermal data, resistivity measurements were also carried out on several sites. The resistivity survey at these sites did not reveal any lateral porosity anomalies along the single profiles, but due to the smooth and continuos layering of the turbiditic sediments, certain features could be tracked in each penetration along the profile. In Fig. 13 all porosity depth profiles of one measurement site are plotted in line to give an overview. Several sections with characteristic gradients or peaks are present in all measurements and marked in grey. Sudden changes from low to high porosity may be an indication for a base of turbiditic deposits. The turbiditic profile of relatively coarse sediment at the base and gradually finer sediment above also is reflected in porosity. Fig. 14 shows a section of a measured porosity profile, which resembles this structure. In this case porosity change amounts to about 15%, this may correspond to a change from silt to clay. The complete section has a thickness of 0.25 m, which agrees well with sediment cores taken near this site during ODP Leg 139, Site 855. The upper part of the core, up to about 10 mbsf, consists of hemipelagic silty clay with interbedded silt turbidites with a sharp basal boundary (Shipboard Scientific Party, 1992).

6. Conclusions

Attached to a heat flow probe, the in situ probe for electrical resistivity complemented well thermal measurements with comparatively little effort and no additional ship time. Due to the implemented acceleration sensor, resistivity–depth profiles, or finally porosity–depth profiles, with vertical resolution of the order of a centimeter could be obtained, in contrast to a vertical resolution of 30 cm for the thermal data. In case of smooth and continuos layering of the sediments, the high resolution allowed a relatively easy assignment of characteristic struc-

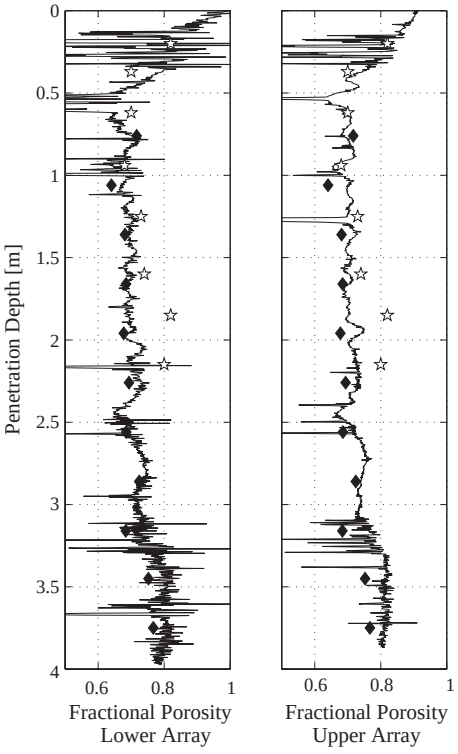

Fig. 12. Porosity versus penetration depth for Profile 56, First Ridge, Penetration 10. Compared are porosities derived from formation factor (solid line), thermal conductivity (solid diamonds), and laboratory data (open stars: gravity core GC40; personal communication, A. Fisher).

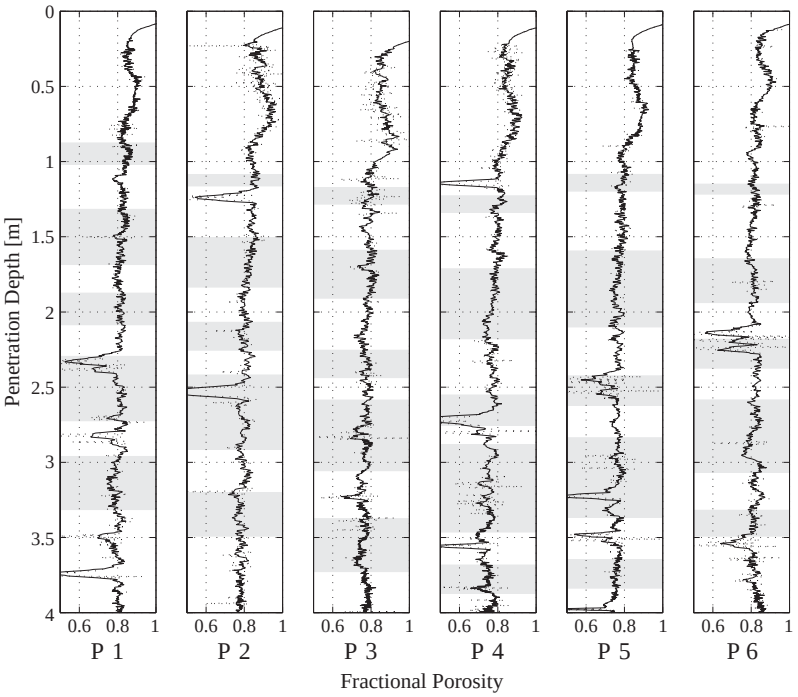

Fig. 13. Porosities of several sites of Profile 60, Middle Valley. The marked sections can be correlated. Dashed line: raw data; solid line: running mean over 10 samples.

tures in the vertical porosity profiles throughout the horizontal profile. This was the case at the Middle Valley measurement site, where certain profile sections may probably be interpreted as silt turbidites,

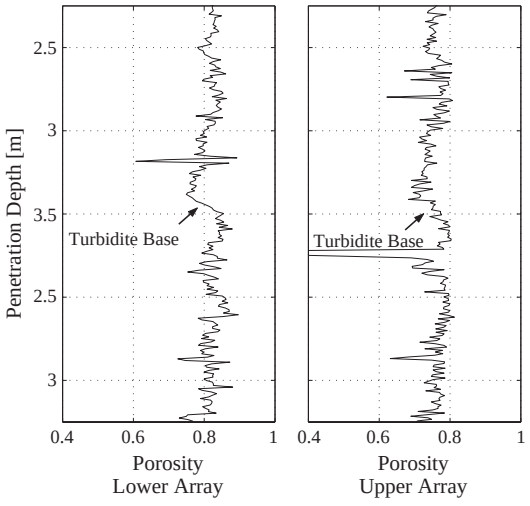

Fig. 14. Part of Profile 60, Penetration 1. The arrow shows a feature which may be interpreted as a turbidity base.

which would be supported by ODP cores taken in the close vicinity. Considering lateral changes of resistivity, the high porosity zones in the vicinity of the forced folds of Fist Ridge could be detected in the resistivity data, although the porosity increase is lower than expected in the uppermost 4 m of sediment, which can be profiled by the in situ probe. Confirmed by independent measurements, the in situ probe proved to be a reliable instrument which allows mapping of near surface porosities of marine deep sea sediments with high vertical resolution at comparatively low cost.

Acknowledgments

We thank all participants and crew members of the cruise SO-149 for the effective collaboration. Furthermore we thank A. Fisher, UCSC, Santa Cruz, USA, and L. Zühlsdorff for providing the sediment core data and the sea floor topography of first ridge, respectively. We also would like to express our thanks to the reviewers W. Brückmann and R. L. Evans. The

research cruise was funded by the German Ministry of Science and Technology with grant 03G0149A.

References

Archie, G.E., 1942. The electrical resistivity log as an aid in determining some reservoir characteristics. Trans. Am. Inst. Min. Metall. Eng. 146, 54–62.

Boyce, R.E., 1968. Electrical resistivity of marine sediments from the Bearing Sea. J. Geophys. Res. 73, 4759–4766.

Brigaud, F., Vasseur, G., 1989. Mineralogy, porosity and fluid control on thermal conductivity of sedimentary rocks. Geophys. J. Int. 98, 525–542.

Bullard, E.C., 1939. Heat flow in South Africa. Proc. R. Soc. Lond., A Math. Phys. Sci. 173, 474–502.

Cosgrove, J.W., Ameen, M.S., 2000. A comparison of the geometry, spatial organization and fracture patterns associated with forced folds and buckle folds. In: Cosgrove, J.W., Ameen, M.S. (Eds.), Forced Folds and Fractures. The Geological Society of London Special Publication, vol. 169, pp. 7–21.

Davis, E.E., Villinger, H., 1992. Tectonic and thermal structure of the middle valley sedimented rift, Northern Juan de Fuca Ridge. In: Davis, E.E., Mottl, M.J., Fisher, A.T. (Eds.), Proc. Initial Reports, ODP Leg 139. Ocean Drilling Program, College Station, TX, pp. 9–41.

Ellis, D.V., 1987. Well logging for Earth scientists. Elsevier.

Hartmann, A., Villinger, H., 2002. Inversion of marine heat flow measurements by expansion of the temperature decay function. Geophys. J. Int. 148 (3), 628–636.

Hyndman, R.D., Davis, E.E., Wright, J.A., 1979. The measurement of marine geothermal heat flow by a multipenetration probe with digital acoustic telemetry and in situ thermal conductivity. Mar. Geophys. Res. 4, 181–205.

Kappel, E.S., Ryan, W.B.F., 1986. Volcanic episodicy and a non-steady state rift valley along Northeast Pacific spreading center: evidence from Sea MARC I. J. Geophys. Res. 91, 13925–13940.

Kinoshita, M., 1994. Estimation of grain thermal conductivity in the turbidite sediment of the Juan de Fuca Ridge. In: Davis, E.E., Mottl, M.J., Fisher, A.T. (Eds.), Proc. Scientific Results, ODP Leg 139. Ocean Drilling Program, College Station, TX, pp. 553–558.

Lister, C.R.B., 1979. The pulse probe method of conductivity measurement. Geophys. J. R. Astron. Soc. 57, 451–461.

McManus, D.A., Holmes, M.L., Carson, B., Barr, S.M., 1972. Late quaternary tectonics, northern end of Juan de Fuca Ridge (northeast Pacific). Mar. Geol. 12, 141–164.

Rosenberger, A., Weidelt, P., Spindeldreher, C., Heesemann, B., Villinger, H., 1999. Design and application of a new free fall in situ resistivity probe for marine deep water sediments. Mar. Geol. 160, 327–337.

Schön, J.H., 1996. Physical properties of rocks: fundamentals and principles of petrophysics. Handbook of Geophysical Exploration, Seismic Exploration, vol. 18. Pergamon Press.

Shipboard Scientific Party, 1992. In: Davis, E.E., Mottl, M.J., Fisher, A.T., et al. (Eds.), Proceedings of the Ocean Drilling Program, Initial Reports, vol. 139. Ocean Drilling Program, College Station, TX.

Shipboard Scientific Party, 1997. Hydrothermal circulation in the oceanic crust and its consequences on the eastern flank of the Juan de Fuca Ridge. In: Davis, E.E., Fisher, A.T., Firth, J.T. (Eds.), Proc. Initial Reports, ODP Leg 168. Ocean Drilling Program, College Station, TX, pp. 7–21.

Spieß, V., Fahrtteilnehmer, 2001. Report and Preliminary Results of RV/Sonne Cruise SO 149, Victoria-Victoria, 16.8. -16.9.2000. Berichte aus dem Fachbereich Geowissenschaften der Universität Bremen, No. 179.

Stearns, D.W., 1978. Faulting and forced folding in the Rocky Mountain foreland. Mem. Geol. Soc. Amer. 151, 1–38.

Villinger, H., Davis, E.E., 1987. A new reduction algorithm for marine heat flow measurements. J. Geophys. Res. 92 (B12), 12846–12856.

Zühlsdorff, L., Spieß, V., submitted for publication. Sedimentation pattern, forced folding and fluid upflow above a buried basement ridge—results from a high resolution seismic 3D survey. J. Geophys. Res.

Zühlsdorff, L., Spieß, V., Hübscher, C., Breitzke, M., 1999. Seismic reflectivity anomalies in sediments at the eastern flank of the Juan de Fuca Ridge: evidence for fluid migration? J. Geophys. Res. 104, 15351–15364.